2.3 Previous Research on Nonlinear Periodic Signal Processing Devices 11 h As explained in the preceding section, nonlinear periodic structures can potentially achieve multiple optical signal processing functions. Considerable past research effort has investigated various	2.3 Các nghiên cứu trước đây về thiết bị xử lý tín hiệu tuần hoàn phi tuyến Như đã nói ở phần trước, các cấu trúc tuần hòa phi tuyến có nhiều tiềm năng trong việc xử lý đồng thời nhiều tín hiệu quang. Trước đây đã có nhiều công trình nghiên cứu các thiết bị xử lý tín hiệu

nonlinear periodic signal processing devices. The theoretical and experimental work is grouped under two categories: solitonic and non-solitonic propagation.

2.3.1 Solitonic Propagation

Studies of pulse propagation in nonlinear Bragg gratings have concentrated on Bragg solitons. Bragg solitons are solitary waves that propagate through a grating without changing their shapes. They arise from the balancing of the dispersion of the grating and the self-phase modulation due to the Kerr nonlinearity, and are predicted theoretically using nonlinear coupled-mode equations. Gap solitons represent the most studied class of Bragg solitons. These are Bragg solitons which have pulse spectra lying entirely within a photonic band gap [17, 18]. The term 'gap soliton' (gap soliton là những sóng phi tuyến lan truyền trong môi trường chiết suất tuyến tính thay đổi tuần hoàn) was first introduced in 1987 by Chen and Mills [19]; then Mills and Trullinger [20] proved the existence of gap solitons by analytic methods. Later, Sipe and Winful [21] and de Sterke and Sipe [22] showed that the electric field satisfies a nonlinear Schrodinger equation, which allows soliton solutions with carrier frequencies close to the edge of the stopband. Christodoulides and Joseph [23], and Aceves and Wabnitz [24] obtained soliton solutions with carrier frequencies close to the Bragg resonance.

Experiments with Bragg gratings have demonstrated soliton propagation, and more importantly, optical switching, and pulse compression. Sankey et al. [25] reported the first observation of all-optical switching in a nonlinear periodic structure using a corrugated silicon-on-insulator waveguide. They showed optical

tuần hoàn phi tuyến khác nhau. Chúng ta có thể chia các công trình thực nghiệm và lý thuyết đó thành hai nhóm: lan truyền soliton và phi soliton.

2.3.1 Lan truyền soliton

Trong các nghiên cứu về lan truyền xung trong cách tử Bragg phi tuyến, người ta thường tập trung vào các soliton Bragg. Các soliton Bragg là sóng đơn độc truyền qua cách tử mà không thay đổi hình dạng. Chúng sinh ra do sự cân bằng giữa hiện tượng tán sắc cách tử và hiện tượng tự điều biến pha do hiệu ứng Kerr, và đã được tiên đoán về mặt lý thuyết bằng các phương trình mode ghép phi tuyến. Các soliton gap là những soliton Bragg được nghiên cứu nhiều nhất. Đây là những soliton Bragg có phổ xung nằm hoàn toàn trong độ rộng vùng cấm photonic [17,18]. Thuật ngữ "soliton gap" do Chen và Mills [19] đưa ra lần đầu tiên; sau đó Mills và Trullinger [20]

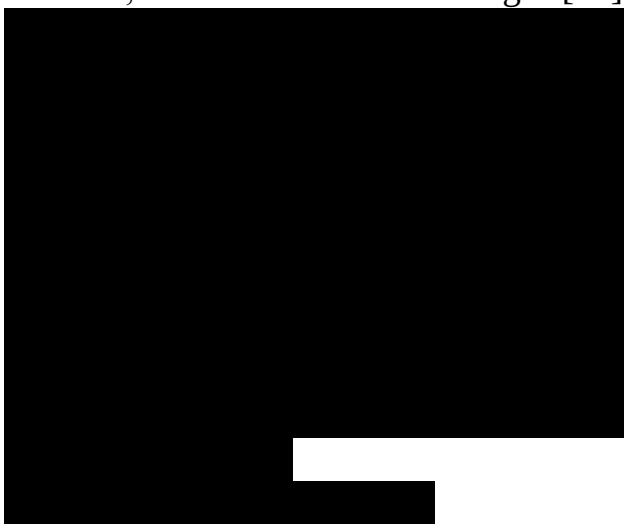

switching of a 5.5 ^J pulse with 50 ns duration at a wavelength A = 1.064 ^m. They demonstrated the concept described in Section 2.2.3 that pulses with frequencies in the stopband are detuned out of the gap because of the nonlinear effects, switching from a highly reflective state to a highly transmissive one. Switching between high- and low-reflectivity states implies these structures can serve as optical switching devices. Soon after Sankey et al., Herbert et al. [8] observed optical power limiting in a three-dimensional colloidal array of microspheres immersed in a Kerr medium. These optical limiters transmit only low-intensity light but block high intensity radiation, and are useful in signal processing functions such as filtering, reshaping, and switching. In 1996, Eggleton et al. [18] reported a direct observation of soliton propagation and pulse compression in uniform fiber gratings, verifying experimentally for the first time the theories developed by Christodoulides and Aceves. This was followed by a further report [26], which both refined the experimental technique and broadened the experimental understanding of the dynamics of pulse propagation in these structures. Pulse compression was also later observed in nonuniform Bragg gratings by Broderick et al. [7]. Optical pulse compression in nonuniform gratings is attributed to two mechanisms: the optical pushbroom effect and cross phase modulation.

The optical pushbroom effect requires a strong optical pump to alter the local refractive index. The pump-induced nonlinear index change creates a

frequency shift at the trailing edge of the probe pulse. The consequent velocity increase of the trailing edge sweeps the probe energy to the front of the pulse, resulting in pulse compression. The change in index due to the pump also acts to detune the weak probe pulse from the center of the band gap, modifying the transmission of the probe [6]. The cross-phase modulation effect works in a similar fashion, except the probe pulse counter-propagates with the signal pulse [7].

2.3.2 Non-solitonic Propagation

Gap solitons are certainly of great interest for applications in telecommunications. However the strict requirements on peak power, pulse shape, and pulse duration needed to balance precisely the effects of dispersion and nonlinearity for producing a soliton may be difficult to satisfy.

Over the past years, studies of non-solitonic pulse propagation through multilayered structures with Kerr-type nonlinearities have attracted considerable attention. Scalora et al. [27] examined the nonlinear propagation of ultrashort pulses through a Kerr nonlinear quarter-wave Bragg reflector. They predicted numerically the possibility of ultrafast optical limiting and switching operations in such a structure. In these operations an increase in the optical field intensity changes the local refractive index due to the material nonlinearity (Eq. 1.1), shifting the entire stopband and making the system transparent at the initial Bragg stopband wavelengths. In order to achieve a higher switching contrast, a nonlinear coupled-cavity-type multilayered structure (NLCC) is proposed by Lee [28]. This new device consists of stacks of two half-wavelength cavity regions sandwiched by standard quarter-wavelength dielectric

mirrors.

In 2000, Brzozowski et al. [9, 14] proposed a novel design of a nonlinear Bragg structure, one that consists of alternating layers of oppositely-signed Kerr materials. Figure 2.3 illustrates the proposed Bragg structure. This device is significantly different from periodic structures studied previously. The key to the novelty is the stability of the device due to the fact the nonlinearity of the structure is balanced precisely. None of the previous periodic structures have such configuration, therefore, they are not inherently stable. Here 'stable operation' means a single output depends solely on a single input (not the case in a bistable device). As a result of the balanced-nonlinearity, the average refractive index n, and thus the Bragg frequency (Eq. 2.3), remain fixed as intensity grows. The behavior of the device does not rely on the movement of stopband edges, but on the establishment of a stopband with intensity-invariant center frequency. Later, Pelinovsky et al. published two thorough theoretical steady-state analyses of this structure [10, 11]. The numerical analyses concluded that the device can perform stable all-optical limiting, even with small time-dependent perturbations [10]. Such optical limiters can be used to filter, shape, and multiplex optical pulses and to limit the optical power [29]. Additionally, optical limiters based on structural resonances - periodic alternations in the Kerr-coefficient - are distinct from other commonly used passive optical limiters exploiting self-focusing, two-photon absorption, and total internal reflection [30]. These limiters provide a usable reflected signal in addition to the transmitted signal. A complete set of logic

functions using the transfer functions of the transmittance and reflectance was proven by Johnson et al. [31].

Figure 2.3: A schematic of a nonlinear Bragg grating with alternating oppositely-signed Kerr coefficients. A is the periodicity of the grating; n01,02 are the linear refractive indices; nnl1,nl2 are the Kerr coefficients of the two adjacent layers.

2.4 Thesis Objective

It is clear from the literature that nonlinear periodic structures represent a promising class of devices to enable a wide range of signal processing operations. Past research has concentrated on either soliton propagation or the steady-state analysis of nonlinear Bragg structures. The switching capabilities of Bragg solitons and the intensity limiting abilities for continuous waves have been studied in detail. However, the temporal behavior of one important class of nonlinear periodic structures - the stable nonlinear periodic devices with constant average refractive index - has been neglected. Furthermore, there has never been a complete investigation contrasting solitonic and non-solitonic propagation behavior in the same device. A systematic study identifying how ultrashort solitonic and non-solitonic pulses are processed in such stable devices remains to be carried out.

Present work considers the temporal behavior of the nonlinear Bragg grating device of Figure 2.3 with a focus on its applications in optical signal processing. The thesis seeks to address the following hitherto unanswered questions:

- in what ways do the proposed nonlinear Bragg structure provide an improvement to optical signal processing

over previously considered devices?

- what are the important design issues in using nonlinear Bragg structures for practical optical signal processing?

- how does the time-dependent (pulse-processing) behavior relate to the known steady- state responses?
- what differentiates solitonic from non-solitonic propagation?

This is the first time-domain analysis of pulse propagation through a stable periodic structure with alternating oppositely-signed Kerr coefficients.

The subsequent chapters will thus characterize both qualitatively and quantitatively the non-solitonic propagation through a nonlinear Bragg structure, and then explore the response of the nonlinear periodic structure model proposed by Brzozowski et al. in the presence of a time-varying incident pulse. The transfer characteristic behavior is expected to be significantly different than that previously revealed through stationary analyses. Furthermore, the large spectral bandwidth of the ultrashort pulses in a time- domain analysis is expected to have further implications on both limiting behavior and pulse distortion.

2.5 Thesis Organization

The organization of the thesis is as follows:

In Chapter 3, the quantitative analytic framework is derived for subsequent deployment throughout the remainder of this thesis. The coupled-mode equations that describe the evolution of pulse envelopes in a nonlinear Bragg grating are derived. The Bragg soliton solutions of these coupled-mode equations are also obtained mathematically in this chapter. Chapter 4 describes the procedure for a

convergent numerical solution of the equations derived. The numerical method for solving the coupled-mode system is explained. The boundary conditions and the balance equations for the system to be satisfied are identified. Also in this chapter, the Bragg structure studied in this thesis is defined and the material parameters chosen for the numerical simulations are stated and justified. Both solitonic (expressions defined in Chapter 3) and non-solitonic pulses are explained. Chapter 5 reports on three sets of time-domain analyses of ultrashort pulse propagation through different Bragg gratings with alternating oppositely-signed Kerr coefficients: (i) 0 linear grating; (ii) in-phase linear grating; (iii) out-of-phase linear grating. The term in-phase linear grating refers to as the case when the material with the higher linear index has a positive Kerr coefficient, and the material with the lower linear index has a negative Kerr coefficient. Similarly, the term out-of-phase linear grating means that the material with lower linear index has a positive Kerr coefficient, and the material with higher linear index has a negative Kerr coefficient. The numerical simulation results and the mechanisms behind the observations are discussed. The thesis concludes in Chapter 6 with an overview of the significant contributions made to optical signal processing and suggests future research directions.

3.4 Exact Soliton Solutions

Since the propagation behavior of solitonic and non-solitonic pulses will be compared in the next chapter, it is important to derive the exact solutions of the coupled-mode system (3.19)-(3.20) for gap solitons. We collaborated with with Professor D. Pelinovsky from McMaster

University to obtain the soliton solutions.

The gap solitons exist in the system when nnl = 0, n0k < 0, n2k > 0, or alternatively when nnl = 0, n0k > 0, n2k < 0. The parameter n2k can be normalized to be positive without loss of generality. In order to find exact solutions for gap solitons when nnl = 0, we adopt relativistic Lorentz transformations of the coordinates, giving:

……

The coupled-mode system (3.19) - (3.20) in these new coordinates then takes the form:

……. (3.23)

Gap solitons are stationary solutions of the coupled-mode system (3.19)-(3.20) that move with a constant velocity V and have a constant detuning frequency (tần số lệch hưởng, độ chênh lệch tần số, độ dịch tần số) Q. Separating variables in the system (3.22)-(3.23), we write these stationary solutions in the form:

a+ = yQZ) ei(^(z)_^(z))+iQr, a_ = ^QC) e^(c)+iQr. (3.24)

The function Q(Z) in (3.24) is the intensity of the right-propagating and left-propagating waves, i.e. Q(Z) = |a+12(Z) = |a_|2(Z), where a±(Z,T) satisfies zero boundary conditions in Z. The functions (0(() - ^(Z)) and ^(Z) in (3.24) are the complex phases of the waves, given that ^(Z) represents the phase difference between the complex phases. It follows from Eqs. (3.22), (3.23), and (3.24) that the functions Q(Z) and ^(Z) satisfy the planar Hamiltonian system:

…… (3.26)

where the Hamiltonian H — H(Q,^) is given by:

H — 2Q (nok + 2n2kQ) cos ^ — 2QQ. (3.27)

The gap soliton solution satisfies the zero boundary conditions at infinity: Q(Z) ^ 0 as |Z| ^ TO. Such solutions occur for H — 0 in Eq. (3.27), requiring:

cos ^ — . (3.28)

The closed-form solution of the system (3.25)-(3.26) can be then written as:

+ U(Q) — 0, where U(Q) — —4Q2 [(nok + 2n2kQ) — ^2] . (3.29)

The system (3.29) describes the zero energy level of a particle moving in a potential field U(Q). The critical point Q — 0 is a saddle point if U"(0) < 0, which necessitates |^| < |nok|. Under this constraint, the trajectory of the solution Q — Q(Z) starts from Q — 0 in the limit Z — —to, grows exponentially until the turning point Q — Qsol, where U(Qsol) — 0, and then decays exponentially to Q — 0 in the limit Z ^ +to. If n2k > 0 and nok < 0, the turning point exists at

The analytical expression for the gap soliton can be derived from Eq. (3.29) and is found to take the form:

…….

where Y — 2(nok — H2)1/2. The gap soliton is centered at Z — 0, where Q(0) — Qsol, and it is exponentially localized, such that Q(Z) ^ Q^e-7|z| as |Z| ^ TO.

The gap soliton solution (Eq. 3.30) exists for n2k > 0, n0k < 0 and 0 = |Q| < |n0k|, i.e., when the nonlinear grating has an out-of-phase built-in modulation of the linear refractive index. The term out-of-phase grating is referred to as the case when the material with the lower linear index has a positive Kerr coefficient, and the material with the higher linear index has a negative Kerr coefficient.

4.1 Introduction

In the previous chapter, the system of coupled-mode equations for nonlinear periodic structures was developed

analytically. This chapter presents the numerical techniques employed in solving the system and asserts the range of physically important material parameters.

4.2 Numerical Method for Solving the CME System

The complex envelope function of the forward and backward propagating waves can be decomposed into its real and imaginary parts:

A+ = u + iw, A_ = v + iy. (4.1)

The real functions u, v, w, and y satisfy the coupled system (3.19) - (3.20), and therefore are given by:

where the nonlinear function /(u,w,v,y) is defined by

/ (u, w, v, y) = nnl(u2 + w2 + 2v2 + 2y2)w + n2k [(u2 + 3w2 + v2 + y2)y + 2uwv]. (4.3)

Assuming the nonlinear functions /(u, w, v, y), /(w, u, y, v), /(v, y, u, w), and /(y, v, w, u) are small, the partial differential equations system in Eq. (4.2) can be further reduced to:

(4.4)

To solve these numerically, a finite-difference method is used, where the functions u, v, w, and y are calculated based on the number of mesh points taken in both time and space:

Z = a ■ Az, where a = 0,1,..., N, N +1, and the space step size Az = ——-;

N + 1

T = /3 ■ At, where ^ = 0,1,..., K, and At is the time step size.

The functions u(Z, T), v(Z, T), w(Z, T), and y(Z, T) can be thought of as two-dimensional vectors, with time and space dimensions. For example, with each element u^A in the array represents the

value of the function u at the grid point (Z = aAz,T = ^At). For simplicity, the term u^z is written as u^ from here on.

The Crank-Nicholson finite difference method is used to solve the partial differential equations defined in Eq. (4.2). The two-dimensional partial differential equations (i.e.,) and)) evaluated at a grid point (Z = aAz,T = /3At) can be approximated as

The partial derivatives of the functions w(Z, T), v(Z, T), and y(Z, T) are approximated in a similar manner. This numerical method is known to be unconditionally stable [11] for any values of At, Az, and n0k. Thus, a linear system is obtained for solving the functions at a specific time instance:

The full derivation of the above linear system is included in Appendix A. The expressions of the matrices A, B, C, D, and H are also stated there.

The complicated coupled-mode system described in Chapter 3 can be now estimated by using the non-iterative algorithm expressed in Eq. (4.7). This makes the numerical computations of the envelope functions u, v, w, and y much simpler.

4.3 Boundary Conditions and Balance Equations

By assumption, the input pulse /in(T) is incident from the left end. The boundary conditions therefore are defined as:

…….. (4.8)

where /in(T) and 0in(T) represent the amplitude and phase modulation of the incident pulse launched at the grating, respectively, at a specific time instance T. Eq. (4.8) can be rearranged by using the relationship in Eq. (4.1) as follows:

…… (4.9)

where /re/ (T) is the intensity of the input

light wave at the input end of the grating (left end), and /tran(T) is the intensity at the output (right end). The reflected and transmitted intensities /re/(T) and /tran(T) are generated dynamically through the time- dependent solutions of the coupled-mode system (3.19)-(3.20).

The boundary conditions defined in Eq. (4.9) are satisfied at all times. In addition to this restriction, the coupled-mode system (3.19)-(3.20) obeys the balance equations:

dT (|.A+|2 + |.A_|2) + dZ (|A+|2 - |A_|2) = 0. (4.10)

Integrating over the nonlinear structure, a balance between the incident, reflected, and transmitted intensities can be obtained:

— I (|A+|2 + |A_|2) dZ = /„„(T) - /r./(T) - WT).

If the incident pulse is fully transmitted and no light becomes trapped within the grating, the conservation of total energy density (W), in the limit T ^ TO, takes the form:

/n(T)dT. (4.11)

where W denotes the total incident, reflected, or transmitted energy density. This balance between total intensities enables the computation of the input-output transmission characteristic for a pulse, Wtran = Wtran(Win).

4.4 The Nonlinear Bragg Structure Model

The device under consideration in this work is a nonlinear Bragg structure which consists of alternating layers of oppositely-signed Kerr materials [9]. This structure was briefly introduced earlier in Chapter 2 (Figure 2.3).

An incident pulse is assumed to be launched at the left end of the structure. The boundary conditions defined in Eq.

4.9 are satisfied at all times. In addition, zero initial conditions are assumed: A±(Z, T = 0) = 0. For most of the simulations, a Gaussian pulse is considered as the input to the system:

……(4.12)

where /peafc is the maximum intensity of the pulse, ^ is the time-delay of the pulse, and a defines the pulse duration as the full width at half maximum, or FWHM:

FWHM = 2a V2 ln2. (4.13)

If ^ ^ FWHM, the pulse intensities approach zero at T = 0 and the small mismatch between the pulse intensity /in(0) and the zero initial condition at T = 0 is neglected.

4.4.1 Material Parameters Justification

This section discusses the physical approximations behind the derivation of the coupledmode system (3.19)-(3.20), and justifies the choice of material parameters n0k and n2k in the numerical modeling of the system.

In deriving the coupled-mode system (3.19)-(3.20), it is assumed that the response time of the optical material is much smaller than the duration of the pulse envelope. Also, in the present work, a maximum index change of 0.01 is assumed. Experimentally, refractive index changes as large as 0.1 have been obtained. Ultrafast index changes have been reported in systems such as polymers doped with azobenzenes, low temperature grown GaAs, or Helium-plasma-assisted molecular beam epitaxy InGaAsP [32, 33, 34, 35]. The response time of the materials was reported to be as fast as 2 ps [33, 34].

In deriving the coupled-mode equations (3.19)-(3.20), the effects of absorption are also neglected. In reality, materials which exhibit index changes as large as 0.1 have

significant linear absorption. Devices made from such highly nonlinear materials would need to be at least two microns thick to give rise to the class of transfer functions considered herein. Over such length a device would lose up to 50% of the transmitted power as a result of absorption. This effect would limit the performance of the optical device. In simulations reported herein, the absorption effects are not included because they do not change the qualitative behavior. It is also noted that index changes of 0.01 can be obtained at spectral points at which the absorption is lowered by orders of magnitude [36].

The specific devices considered herein assume significant control over the values of both the Kerr coefficient (oppositely-signed) and linear indices of the materials. In a two- level system with a single absorption resonance, the sign of the Kerr coefficient is positive for wavelengths shorter than the wavelength of maximum absorption and for wavelengths longer than the wavelength of maximum two-photon absorption [16]. For wavelengths in between these two regions the sign of Kerr coefficient is negative [37]. Thus, for any two nonlinear materials with single absorption resonances at different spectral positions there exists a spectral range where the Kerr nonlinearities are of opposite sign. Also, index- matching techniques can be used to enable control over the value of the linear index. For example, a combination of polymers in correct proportions can be used in organic systems in order to obtain the desired bulk refractive index. In the case of compound semiconductors, a change in the composition tunes the linear refractive index.

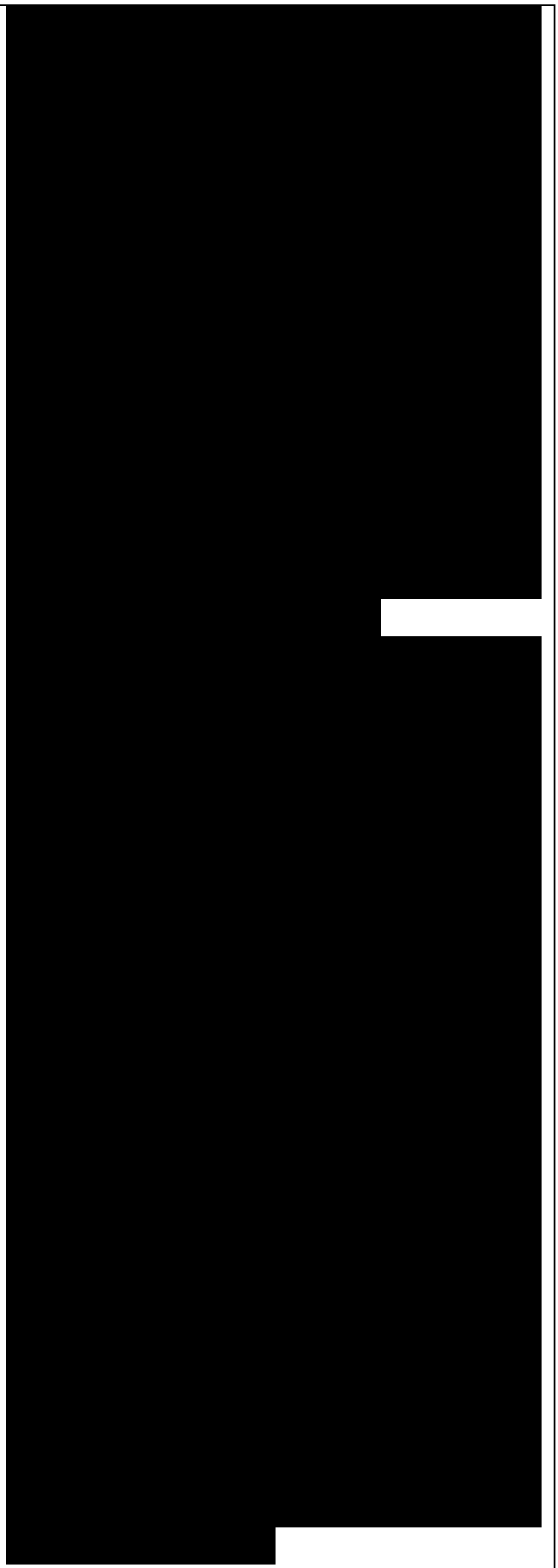

Throughout the simulations reported herein, the Kerr coefficients nrall>2 of the two adjacent layers are assumed to be nnll,2 = ±2.5 x 10-12 cm2/W, and the average linear index nln = (n0l + n02)/2 is fixed at 1.50. The center frequency of the incident pulse is assumed fixed at f0 = 2x 10l4 Hz (or at wavelength A0 = 1.50 ^m). These choices give the values nnl = 0 and n2k = 2- x 10-11 cm2/W in the coupled-mode system (3.19)-(3.20).

4.5 Numerical Model Validation and First Explo-ration

This section describes the evolution of pulse shape and spectrum when short optical pulses propagate through the nonlinear Bragg structure. In general, Kerr nonlinearity- induced self-phase modulation and grating-generated dispersion occur simultaneously, and both tend to modify the shapes of the propagating optical pulses. However, under certain circumstances, an exact cancellation of these two effects can occur, allowing the Bragg soliton to propagate through large distances with no change in shape. Given the availability of the analytical solutions of the Bragg soliton, the simulations presented in this section serve to validate the numerical model.

In Section 3.3, the soliton solutions to the coupled-mode system were derived. The propagation of a Bragg soliton with its shape defined in Eq. (3.30) is simulated here to compare with its known properties to validate the numerical model. Device parameters of nnl = 0, n2k = 2L x 10-11 cm2/W, and n0k = —0.1 are used in the coupled-mode system (3.19) -(3.20).

The parameters of the Bragg solitons are chosen as: /peak = 55 GW/cm2, input soliton pulse FWHM « 27 fs, the constant velocity factor V = 0.5, and the detuning

frequency Q = 0.01. The intensities of the forward and backward waves |A±|2 for a propagating Bragg soliton are simulated and shown in Figure 4.1(a) and 4.1(b) below. The Bragg soliton propagates with a constant speed V and a constant detuning

(b)

Figure 4.1: Bragg soliton propagation simulated using the system (3.19)-(3.20) with nn1 = 0, n0k = -0.1, and n2k = 2L x 10_11 cm2/W. Shown are (a) the intensity of the forward wave and (b) the intensity of the backward wave. The parameters of the Bragg soliton are: /peak = 55 GW/cm2 and FWHM « 27 fs.

frequency Q from the center of the stopband frequency w0. The amplitude envelope of both forward and backward propagating waves remain constant spatially. Thus steady propagation of Bragg solitons is observed in devices with large L.

For comparison, the propagation of a non-solitonic pulse (a Gaussian pulse defined in Eq. 4.12) with Ipeak = 55 GW/cm2 and FWHM = 27 fs through the same device is simulated to illustrate the effect of imbalance between self-phase modulation and dispersion. Two scenarios of Gaussian pulse propagation are observed, depending on the parameter n0k which represents the strength of the linear index grating along the structure. If n0k = 0, the pulse amplitude decays and the pulse width grows over the propagation distance. This scenario is shown in Figure 4.2. If n0k = —0.1 (the same device as in the soliton case in Figure 4.1), the pulse amplitude experiences strong compression, pulse reshaping and high-amplitude multiple-peak oscillations. This scenario is shown in Figure 4.3. Pulse compression-decompression cycling is observed in the

system (3.19) -(3.20) in the case when n0k < 0 (Bragg soliton propagation is possible); and pulse amplitude decay is observed when n0k > 0 (Bragg soliton propagation is not allowed).

To summarize, a gap soliton (Eq. 3.24) propagates through the periodic structure as a uniformly shaped soliton pulse in both coupled counter-propagating waves. When a non-solitonic pulse (Eq. 4.12) is launched at the input of the optical device, it could also evolve into a gap soliton. In the case when the system does not support solitons, pulse propagates as a forward wave, generates a reflected backward wave, therefore exhibits non-solitonic behavior: the pulse amplitude decays, or the pulse compresses, gets reshaped and oscillates.

(b)

Figure 4.2: Decaying Gaussian pulse propagates in the same structure as in Figure 4.1, but without a built-in linear grating (n0k = 0). Shown are (a) the intensity of the forward wave and (b) the intensity of the backward wave. The parameters of the Gaussian pulse are: /peak = 55 GW/cm2 and FWHM = 27 fs to match the Bragg soliton in Figure 4.1.

Figure 4.3: Gaussian pulse propagates in structure with an out-of-phase built-in linear grating (n0k = -0.1). Compression-decompression cycling is observed. All other parameters are the same as in Figure 4.2. Shown are (a) the intensity of the forward wave, (b) the intensity of the backward wave, (c) top view of (a), and (d) top view of (b).